Available online at www.sciencedirect.com

SciVerse ScienceDirect

Ceramics International 39 (2013) 3721–3729

CERAMICS INTERNATIONAL

www.elsevier.com/locate/ceramint

Structure, dielectric and ferroelectric properties of $0.92Na_{0.5}Bi_{0.5}TiO_3$–$0.06BaTiO_3$–$0.02K_{0.5}Na_{0.5}NbO_3$ lead-free ceramics: Effect of Co_2O_3 additive

H.Y. Ma[a], X.M. Chen[a,*], J. Wang[a], K.T. Huo[a], H.L. Lian[b], P. Liu[a]

[a]*College of Physics and Information Technology, Shaanxi Normal University, Xi'an 710062, PR China*
[b]*School of Science, Xi'an University of Posts and Telecommunications, Xi'an, 710121, PR China*

Received 11 October 2012; received in revised form 16 October 2012; accepted 16 October 2012
Available online 23 October 2012

Abstract

$0.92Na_{0.5}Bi_{0.5}TiO_3$–$0.06BaTiO_3$–$0.02K_{0.5}Na_{0.5}NbO_3$+$x$ wt% Co_2O_3 (NBKT–xCo, x=0, 0.2, 0.4, 0.6, 0.8) lead-free ferroelectric ceramics were prepared via a conventional solid state reaction method. Effects of Co_2O_3 additive on crystallite structure, microstructure, dielectric and ferroelectric properties of the NBKT–xCo ceramics were studied. X-ray diffraction results showed that the rhombohedral–tetragonal morphotropic phase boundary existed in all the ceramics, with relative amount of tetragonal phase varying with the content of Co_2O_3. Average grain size, maximum value of dielectric constant, Curie temperature and ferroelectric properties of the ceramics were close related to the content of Co_2O_3. The dielectric anomaly caused by the phase transition between the ferroelectric phase and the so-called "intermediate phase" was observed in the ceramics with $x \leq 0.2$, while it disappeared with further increasing x. All the ceramics showed a diffuse phase transition between the "intermediate phase" and the paraelectric phase. The change in the ferroelectric properties with changing the content of Co_2O_3 was discussed by considering the competitive effects among grain size, relative amount of the tetragonal phase and oxygen vacancies.

Keywords: B. Electron microscopy; B. X-ray methods; C. Dielectric properties; C. Ferroelectric properties

1. Introduction

Lead-free ceramics have been studied widely in recent years owing to the environmental protection concerns. Among various lead-free ferroelectric ceramics, $(1-x)Na_{0.5}Bi_{0.5}TiO_3$–$xBaTiO_3$ (NBT–xBT)-based ceramics have attracted considerable attention on account of the existence of a rhombohedral–tetragonal morphotropic phase boundary (MPB) near x=0.06 [1–5]. Compared with pure $Na_{0.5}Bi_{0.5}TiO_3$ ceramics, the NBT–xBT ceramics near the MPB have much better piezoelectric and ferroelectric properties [6,7]. In our previous work, we found that doping of $BiFeO_3$, sintering atmosphere, and Na nonstoichiometry all affected structure and electrical properties of the NBT–0.06BT lead-free ceramics obviously, which was related to the formation of oxygen vacancies and/or cation vacancies in the ceramics [8–10]. The incorporation of $(K_{0.5}Na_{0.5})NbO_3$ (KNN) in NBT–xBT-based ceramics can also improve electrical properties of the ceramics. Zhang et al. reported a giant strain in the NBT–BT–KNN system [11]. Gao et al. observed a temperature and frequency independent energy-storage property [12]. The ferroelectric and piezoelectric properties of the NBT–BT–KNN ceramics could be further ameliorated by using donor and/or acceptor dopants, as well as controlling the formation of defects in the ceramics [13].

As an additive, cobalt oxide has been found to be effectual in improving the electrical properties of NBT-based ceramics. Xu et al. reported that the doping of CoO in NBT–0.07BT ceramics could elevate its depolarization temperature [14]. Jiang et al. observed that the addition of Co_2O_3 in NBT–0.08BT ceramics could eliminate the phase transition from the ferroelectric state to the "antiferroelectric state" [15]. Hu et al. found that depolarization temperature and piezoelectric property of Co_2O_3-added–NBT–BT–$(Bi_{0.5}K_{0.5})TiO_3$ ceramics were related to the

*Corresponding author. Tel./fax: +86 29 81530750.
E-mail address: xmchen@snnu.edu.cn (X.M. Chen).

0272-8842/$ - see front matter © 2012 Elsevier Ltd and Techna Group S.r.l. All rights reserved.
http://dx.doi.org/10.1016/j.ceramint.2012.10.208

acceptor doping behavior of Co_2O_3 [16]. However, to our knowledge, effects of Co_2O_3 on crystallite structure, microstructure and dielectric and ferroelectric properties of NBT–BT–KNN systems have not been fully clarified.

In this work, Co_2O_3-added–$0.92Na_{0.5}Bi_{0.5}TiO_3$–$0.06BaTiO_3$–$0.02K_{0.5}Na_{0.5}NbO_3$ lead-free ferroelectric ceramics were fabricated via a conventional solid state reaction method. The effect of Co_2O_3 on crystallite structure, microstructure, dielectric, and ferroelectric properties of the ceramics were studied in detail.

2. Experimental procedure

$0.92Na_{0.5}Bi_{0.5}TiO_3$–$0.06BaTiO_3$–$0.02K_{0.5}Na_{0.5}NbO_3+x$ wt% Co_2O_3 (NBKT–xCo, $x=0$, 0.2, 0.4, 0.6, 0.8) lead-free ceramics were prepared via a conventional solid state reaction method. The starting raw materials were Na_2CO_3 ($\geq$99.8%), $BaCO_3$ ($\geq$99.0%), K_2CO_3 ($\geq$99.0%), Bi_2O_3 ($\geq$98.9%), TiO_2 ($\geq$98.0%), Nb_2O_5 ($\geq$99.5%) and Co_2O_3 ($\geq$99.0%). All raw materials were baked at 100 °C for 24 h in order to remove water content, and then weighed immediately according to the chemical formula. The powders were milled in agate vials with agate balls for 24 h using alcohol as a medium in a planetary ball milling system. After drying, the milled powders were calcined at 920 °C for 3 h. The calcined powders were milled again for 12 h and then pulverized with approximately 5 wt% polyvinyl alcohol. Pellets of 11.5 mm in diameter and approximately 1.5 mm in thickness were pressed at a uniaxial pressure of 200 MPa and burned out the binder at 500 °C for 2 h. The pellets were sintered at 1150 °C for 3 h in air. Heating and cooling rates were 3 °C/min. In order to prevent volatilization of Bi^{3+}, K^+ and Na^+ ions, all pellets were embedded in powders with the same composition and placed in covered alumina crucibles during the sintering process.

Bulk density of the ceramics was measured by the Archimedes method. X-ray diffraction (XRD, Rigaku D/Max 2550) in a step mode using a Cu K_α radiation was used for identification of phase compositions. For powder XRD measurement, the ceramics were crushed into fine powder and annealed at 400 °C for 3 h in covered alumina crucibles in order to thermally anneal residual stresses induced by the grinding process. The measurements were made at 40 kV and 100 mA with a step size of 0.01° and 2 s/step. Additionally, in order to examine the XRD peaks at 46.5° more precisely, data were collected in the 2θ range of 46.2–46.8° with a scanning step of 0.004° and 6 s/step. Scanning electron microscopy (SEM) was performed with a scanning electron microscope (Quanta 200, FEI Co., Eindhoven, Netherlands). Average grain size was determined by the line intersect method.

In order to characterize dielectric and ferroelectric properties of the ceramics, silver electrodes were coated and fired at 650 °C for 20 min. Dielectric measurement was performed with a precision LCR meter (Agilent E4980A) from room temperature to 400 °C. Ferroelectric hysteresis loops were measured at 50 Hz and room temperature in a silicon oil with a radiant precision workstation ferroelectric testing system.

3. Results and discussion

XRD patterns of the NBKT–xCo ceramics are shown in Fig. 1(a). All ceramics exhibit typical ABO_3 perovskite diffraction peaks and no secondary phase is observed, suggesting that NBKT and Co_2O_3 have formed a solid solution with the perovskite structure or the secondary phase cannot be detected within the precision limit of the X-ray diffractometer. As we know, a rhombohedral–tetragonal MPB exists in NBT–BT -based ceramics [6], so that the XRD peaks at about 46.5° are characterized with the presence of (002) and (200) peaks corresponding to the tetragonal phase and (200) peak corresponding to the rhombohedral phase [17]. Detailed XRD patterns at about 46.5° are shown in Fig. 1(b–f). All peaks are asymmetrical. To characterize the phase compositions in a more quantitative way, the peaks were fitted by Peakfit software using the least-square approach. In order to obtain minimum values of residual error, the peak shape was modeled by a Pearson-VII function taking into account both Lorentzian and Gaussian functions. The fitting of the peaks showed a quick convergence by considering both the perovskite-type tetragonal phase and rhombohedral phase. The peaks were fitted into $(002)_T$, $(200)_T$ and $(200)_R$ peaks for all the ceramics, where T and R denote the tetragonal and rhombohedral phase, respectively. The results indicate that the MPB appears in all the samples. By using $T\% = (Area_{(002)T} + Area_{(200)T})/(Area_{(002)T} + Area_{(200)T} + Area_{(200)R})$, percentage of the tetragonal phase T% was determined to be about 31.0%, 32.3%, 34.1%, 40.2% and 26.7% for the NBKT–xCo ceramics with $x=0$, 0.2, 0.4, 0.6 and 0.8, respectively.

Fig. 2(a–e) demonstrates surface SEM images of the NBKT–xCo ceramics. All ceramics show similar fractures. A typical SEM micrograph of fractured surface of the sample with $x=0.2$ is shown in Fig. 2(f). Almost no pores are observed in all the ceramics, suggesting that they were well sintered. Bulk densities of the ceramics are about 5.73 g cm^{-3}, corresponding to a relative density of higher than 94%. By means of the linear intercept method, mean grain sizes of the ceramics with $x=0$, 0.2, 0.4, 0.6, and 0.8 were determined to be about 1.0, 1.3, 1.8, 2.0 and 1.9 μm, respectively. The average grain size of the ceramics increases with the increase in the amount of Co_2O_3 up to $x=0.6$. As is generally recognized, the segregation of oxide additives at grain boundaries can inhibit grain growth [18]. Therefore, the increase in the grain size of the ceramics suggests that Co_2O_3 has dissolved into the perovskite structure, which is in accordance with the XRD results. On the other hand, oxygen vacancies would be created to maintain overall electrical neutrality due to the substitution of Co^{3+} ions for Ti^{4+} ions. The formation of oxygen vacancies in oxides is beneficial to mass transport during sintering, which causes an increase in grain size [19]. Previously, we found that NBT–xBT-based ceramics with higher oxygen vacancy concentration had larger grains [9]. Thus, oxygen vacancies in the

NBKT–xCo ceramics should be responsible for the promoted grain growth.

Fig. 3 shows dielectric constant (ε_r) and dielectric loss (tan δ) of the NBKT–xCo ceramics as a function temperature (T). For the ceramics with $x=0$ and 0.2, two dielectric anomalies are observed distinctly in the ε_r–T curves (Fig. 3a–b). The first dielectric anomaly appears at about 170 °C (denoted as T_d), which is traditionally attributed to the phase transition between the ferroelectric phase and the so-called "anti-ferroelectric phase", due to the appearance of double hysteresis loops above T_d [6]. However, this has not been confirmed by other experimental measurements [20–22]. It has also reported that the double hysteresis loops may be associated with subtle modulation of spontaneous polarization [23], electromechanical interaction between the polar and non-polar regions [24], macro–micro domain switching [25], and so on. Therefore, the first dielectric anomaly near T_d is widely considered to be caused by the phase transition from the ferroelectric phase to a so-called "intermediate phase" [26,27]. As temperature is lower than T_d, ε_r at higher frequency is lower than that at lower frequency. ε_r at different frequencies merges together with increasing temperature above T_d. The second dielectric anomaly corresponding to the maximum value of ε_r (denoted as ε_m) locates at Curie temperature (T_m), which is related to the phase transition between the so-called "intermediate phase" and the paraelectric phase. As temperature is higher than T_m, ε_r drops with increasing temperature. For the NBKT–xCo ceramics with $x=0.4$, 0.6 and 0.8, the first dielectric anomaly disappears and only the dielectric peak located at T_m is observed (Fig. 3c–e). Similar phenomenon was also

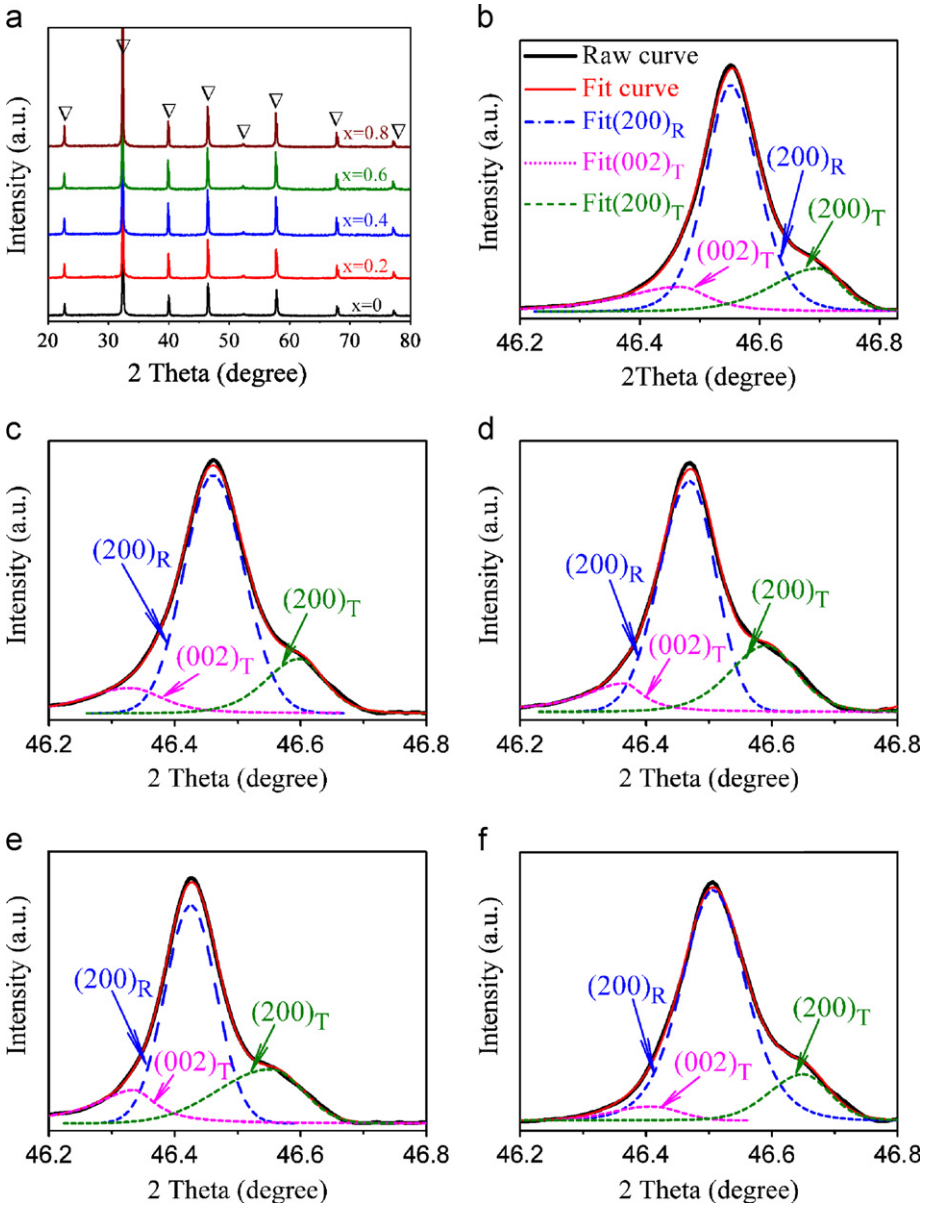

Fig. 1. XRD patterns of the NBKT–xCo ceramics (a), and their XRD fitting patterns over 46.2°–46.8°: (b) $x=0$, (c) $x=0.2$, (d) $x=0.4$, (e) $x=0.6$, and (f) $x=0.8$.

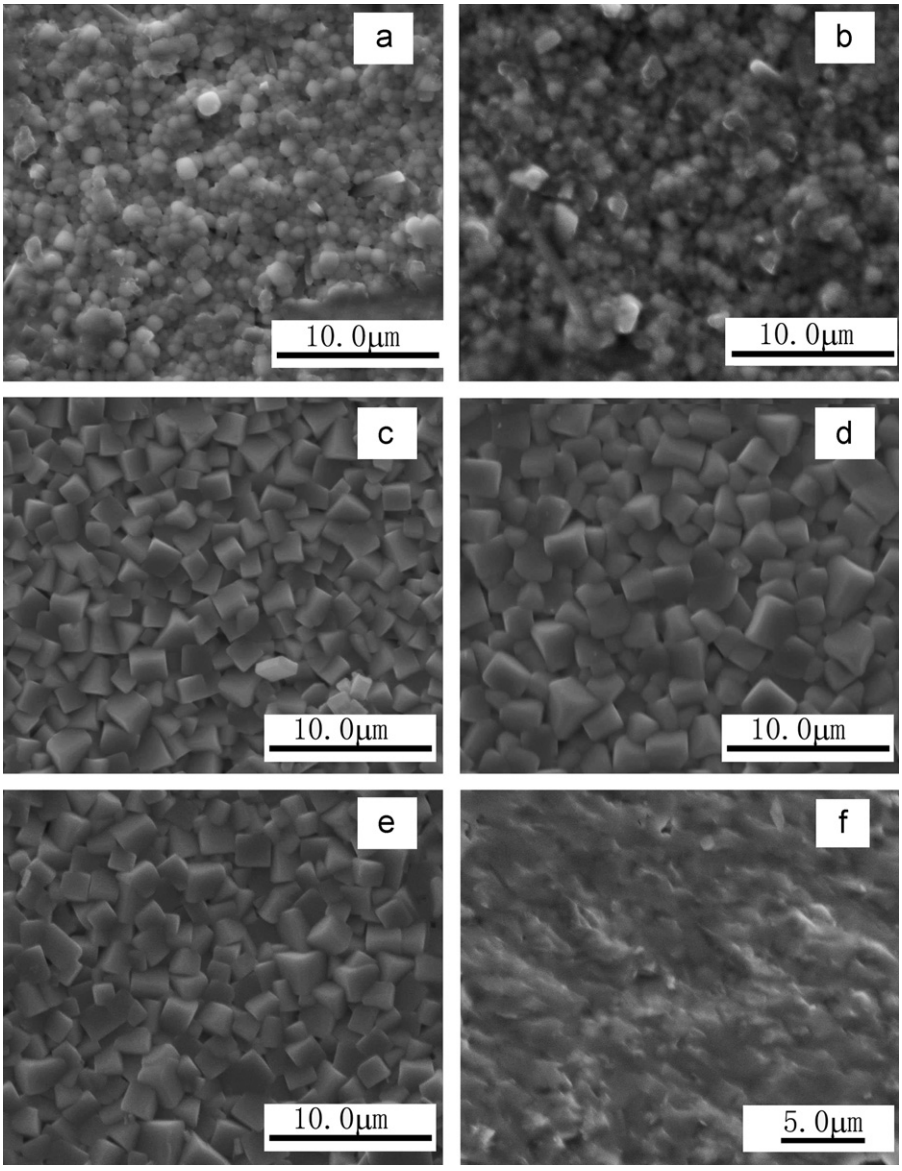

Fig. 2. Surface SEM images of the NBKT–xCo ceramics with (a) $x=0$, (b) $x=0.2$, (c) $x=0.4$, (d) $x=0.6$, (e) $x=0.8$; and (f) SEM image of fractured surface of the NBKT–0.2Co ceramic.

observed in our previous work on the NBT–xBT-based ceramics sintered in nitrogen atmosphere [9]. Either the substitution of Co^{3+} for Ti^{4+} in the NBKT–xCo ceramics here or sintering the ceramics in nitrogen atmosphere previously, could create oxygen vacancies in the ceramics. As we know, oxygen vacancies can cause domain wall clamping, which will inhibit the transition between the ferroelectric phase and the so-called "intermediate phase" [28]. As a result, the disappearance of the first dielectric anomaly for the NBKT–xCo ceramics with $x \geq 0.4$ could attributed to oxygen vacancy effect.

The values of ε_m and T_m measured at 100 kHz are listed in Table 1. The ε_m value increases with the increasing amount of Co_2O_3. As mentioned above, with increasing Co_2O_3, oxygen vacancy concentration increases. That is to say, the ceramics with higher oxygen vacancy concentration have higher ε_m values, which is always related to electron relaxation polarization [29]. Similar phenomena were also observed in Mn-doped $SrTiO_3$ and $(BaCa)(TiZr)O_3$ ceramics [29,30]. In addition, for most polycrystalline ferroelectric ceramics with grain size in the range of 1–5 μm, there is a decrease in the dielectric constant with decreasing grain size [31]. So, the increase in grain size of the NBKT–xCo ceramics from about 1.0 μm to about 2.0 μm also contributed to the increase in ε_m. The T_m value decreases as x is increased from 0 to 0.6 and then increases at $x=0.8$. It has been reported that a change in phase transition temperature is associated with many factors, such as defect concentration [32,33], crystallite structure [34], grain size [35] and secondary phase [36]. Uchino et al. found that the Curie temperature of $BaTiO_3$ was affected by grain size as the size was less than 200 nm [35]. Here, the average grain

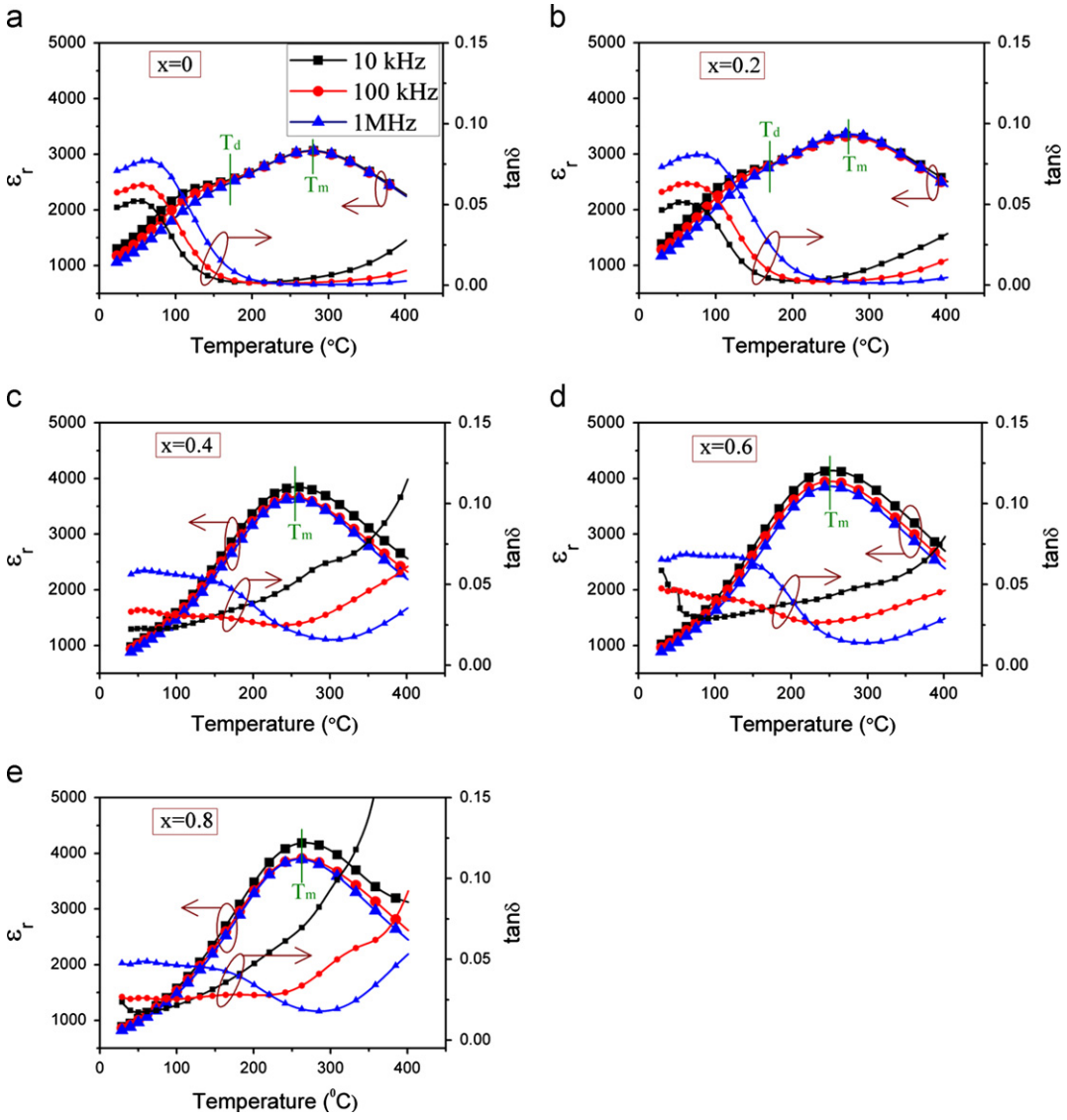

Fig. 3. Dielectric constant and dielectric loss of the NBKT–xCo ceramics versus temperature at frequencies of 10 kHz, 100 kHz and 1 MHz.

Table 1
Dielectric and ferroelectric properties of the NBKT–xCo ceramics.

	$x=0$	$x=0.2$	$x=0.4$	$x=0.6$	$x=0.8$
ε_m (100 kHz)	3054	3317	3664	3948	4758
T_m (°C, 100 kHz)	278	272	253	251	266
P_m (μC/cm^2, 55 kV/cm)	13.6	10.9	20.3	23.1	21.5
P_r (μC/cm^2, 55 kV/cm)	5.0	4.2	15.2	21.1	21.0
E_c (kV/cm, 55 kV/cm)	16.1	16.9	22.6	24.1	26.2

sizes of the ceramics are far larger than 200 nm. Therefore, it is unlikely that the change in grain size is responsible for the variation in T_m. Secondary phase can also cause a change in T_m [36], but no secondary phase was observed in the present study (Fig. 1a). In our previous work, we found that the T_m of the NBT-based ceramics was closely related to the concentration of oxygen vacancies and the percentage of tetragonal phase [9]. Here, both the percentage of the tetragonal phase and oxygen vacancy concentration were changed with the Co_2O_3 amount. Therefore, the difference in T_m among the ceramics with different Co_2O_3 contents can be attributed to the competitive effect between the oxygen vacancy concentration and the relative amount of tetragonal phase. However, which factor played a more important role is unclear currently, which will be further studied in our future work.

The ε_r–T curves of the NBKT–xCo ceramics exhibit broad dielectric peaks around the Curie temperature, which is a characteristic of diffuse phase transition. The dielectric behaviors were further studied by fitting the results to the modified Curie–Weiss law, which is given by [37]: $(1/\varepsilon_r)-(1/\varepsilon_m)=(T-T_m)^\gamma/C$, where ε_m is the maximum value of dielectric constant at the phase transition temperature T_m, C is Curie-like constant, and γ is the degree of diffuseness. γ is usually ranging from 1 for a normal ferroelectric to 2 for an ideal relaxor ferroelectric.

Plots of $\mathrm{Ln}((1/\varepsilon_r)-(1/\varepsilon_m))$ as a function of $\mathrm{Ln}(T-T_m)$ for all samples at 10 kHz are shown in Fig. 4. By least-square fitting the experimental data to the modified Curie–Weiss law, γ was obtained. γ values of the NBKT–xCo ceramics with $x=0$, 0.2, 0.4, 0.6 and 0.8 were determined to be about 1.96, 2.00, 1.99, 2.02 and 1.92, respectively. Because the diffuseness exponent γ of all the samples is close to 2, the phase transition shows a diffuse character. In the NBKT–xCo ceramics, four kinds of ions, Na^+, Bi^{3+}, K^+ and Ba^{2+}, occupy A-site; Ti^{4+} and Nb^{5+} ions occupy B-site. These cations in the A-site or B-site possess similar radii but different charges. The diffuse phase transition behavior of the ceramics is always related to the co-existence of the A-site and/or B-site complex cations [38].

Fig. 5 shows polarization of the NBKT–xCo ceramics vs. electric field measured at 50 Hz and room temperature. In order to obtain the saturated polarization characterization, the specimens were measured at 40–55 kV/cm. It is found that the constricted polarization hysteresis loops tend to be saturated curves with increasing amount of Co_2O_3. The remnant polarization (P_r), maximum polarization (P_m) and coercive field (E_c) of the ceramics measured at 55 kV/cm are listed in Table 1. The ceramics with $x=0$ and 0.2 show lower P_m, P_r and E_c values, compared with the ceramics with $x=0.4$, 0.6 and 0.8. The values of polarization and coercive field vary with the amount of Co_2O_3.

In our previous work, we found that the ferroelectric properties of the NBT -based ceramics were determined by competitive factors, such as crystallite structure, grain size and defects [8–10]. Here, the relative amount of tetragonal phase in the NBKT–xCo ceramics increases from $x=0$ to 0.6, which could enhance the ferroelectric properties to some extent [39]. In addition, as grain size is about or less

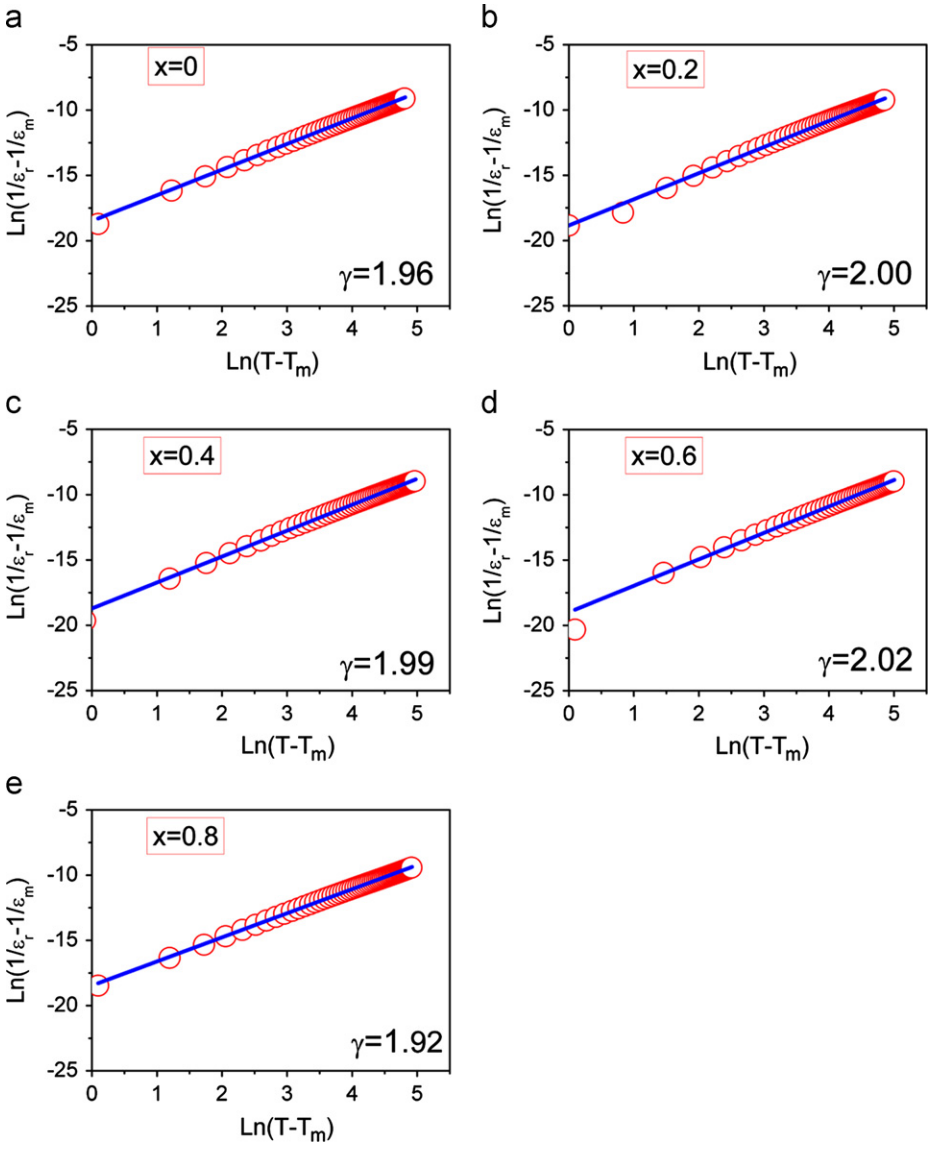

Fig. 4. Plots of $\mathrm{Ln}(1/\varepsilon_r-1/\varepsilon_m)$ vs. $\mathrm{Ln}(T-T_m)$ for the NBKT–xCo ceramics at the frequency of 10 kHz. The symbols denote experimental data, while the solid lines denote the least-squared fitting curves to the modified Curie–Weiss law.

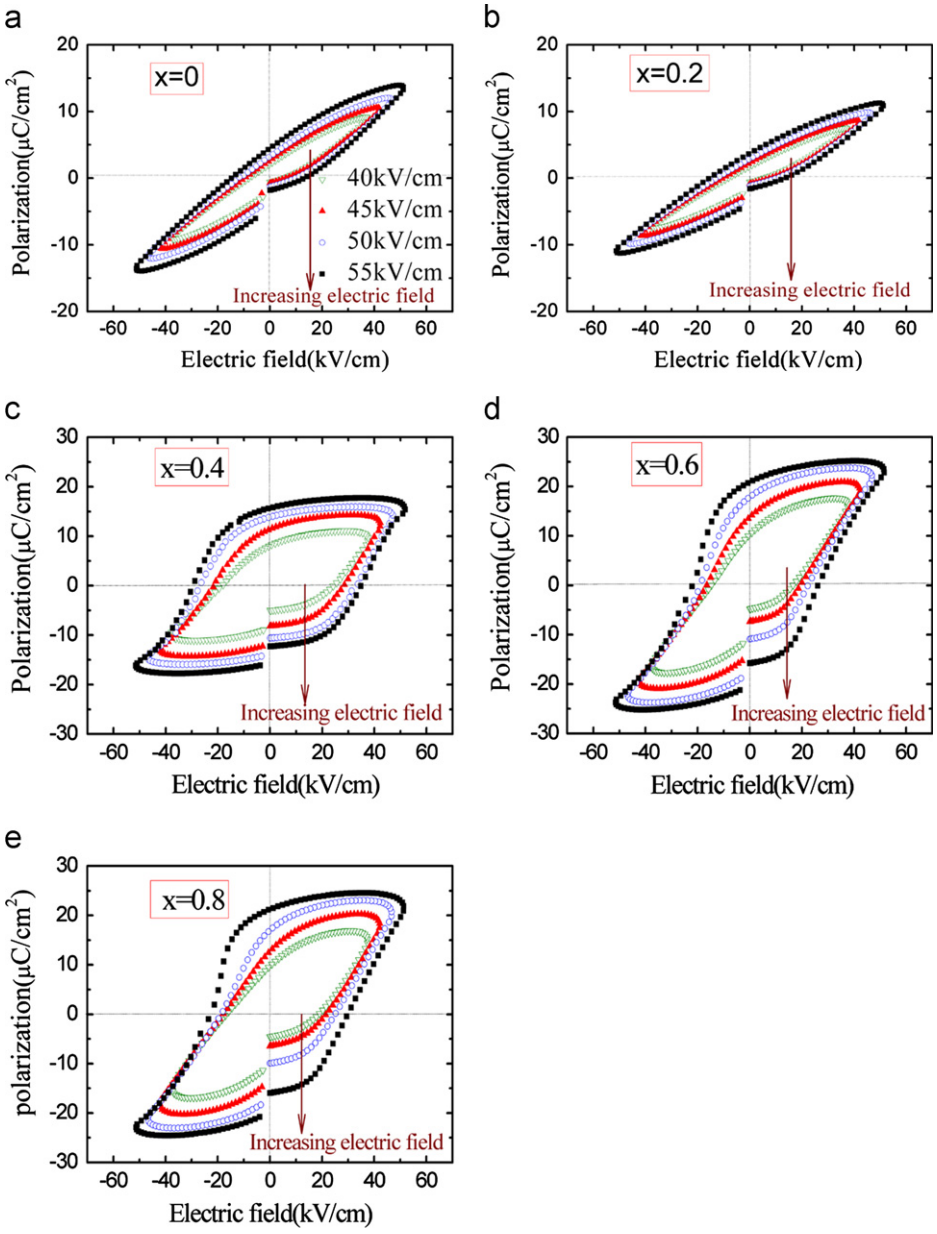

Fig. 5. *P–E* loops of the NBKT–*x*Co ceramics.

than 1 μm, the coupling between grain boundaries and domain walls is strong, which can weaken the ferroelectric properties of the ceramics [40]. The NBKT–*x*Co ceramics with $x=0$ and 0.2 have smaller average grain sizes, while the mean grain sizes of the ceramics with $x=0.4$, 0.6 and 0.8 are larger than 1 μm. Therefore, it can be expected that the ceramics with $x=0$ and 0.2 show weakened ferroelectric properties from the viewpoint of the grain size effect. The substitution of Co^{3+} ions for Ti^{4+} ions caused oxygen vacancies. To our knowledge, oxygen vacancies are unfavorable to polarization switching, leading to a decrease in P_r and increase in E_c [41]. Therefore, the difference in ferroelectric properties among the ceramics with different Co_2O_3 amounts should be a result of the competitive effects among grain size, relative amount of tetragonal phase and oxygen vacancies.

4. Conclusions

Effects of Co_2O_3 on crystallite structure, microstructure, dielectric and ferroelectric properties of the NBKT–*x*Co lead-free ferroelectric ceramics were studied. The NBKT–*x*Co ceramics, with $x=0$, 0.2, 0.4, 0.6 and 0.8, had relative amounts of tetragonal phase of 31.0%, 32.3%, 34.1%, 40.2% and 26.7%, and the mean grain sizes of 1.0, 1.3, 1.8, 2.0 and 1.9 μm, respectively. ε_m and T_m values also changed with the Co_2O_3 content. An obvious dielectric anomaly, corresponding to the phase transition between ferroelectric phase and the so-called "intermediate phase" was observed in the NBKT–*x*Co ceramics with $x=0$ and 0.2, while it disappeared in the samples with higher contents of Co_2O_3. All the ceramics showed a diffuse character of phase transition between the "intermediate

phase" and the paraelectric phase. The variation in ferroelectric properties of the ceramics with the Co_2O_3 content was a result of the competitive effects among grain size, relative amount of the tetragonal phase and oxygen vacancies.

Acknowledgments

This work was supported by the National Natural Science Foundation of China (No. 11004127), Shaanxi Province Science and Technology Foundation (No. 2012KJXX-30), Xi′an Science and Technology Foundation (No. CXY1009 (1)), Fundamental Research Funds for the Central Universities (No. GK200902054) and Innovation Funds of Graduate Programs, Shaanxi Normal University (Grant no. 2012CXS032).

References

[1] M. Cernea, E. Andronescu, R. Radu, F. Fochi, C. Galassi, Sol–gel synthesis and characterization of $BaTiO_3$-doped $(Bi_{0.5}Na_{0.5})TiO_3$ piezoelectric ceramics, Journal of Alloys and Compounds 490 (2010) 690–694.

[2] M.L. Liu, Y.F. Qu, D.A. Yang, Effect of Bi_2O_3 doping methods on the positive temperature coefficient property of $Ba_{0.999}(Bi_{0.5}Na_{0.5})_{0.001}TiO_3$ ceramics, Journal of Alloys and Compounds 503 (2010) 237–241.

[3] P. Fu, Z.J. Xu, R.Q. Chu, W. Li, G.Z. Zang, J.G. Hao, Piezoelectric, ferroelectric and dielectric properties of Nd_2O_3-doped $(Bi_{0.5}Na_{0.5})_{0.94}Ba_{0.06}TiO_3$ lead-free ceramics, Materials Science and Engineering B 167 (2010) 161–166.

[4] Y.J. Dai, S.J. Zhang, T.R. Shrout, X.W. Zhang, Piezoelectric and ferroelectric properties of Li-doped $(Bi_{0.5}Na_{0.5})TiO_3$–$(Bi_{0.5}K_{0.5})TiO_3$–$BaTiO_3$ lead-free piezoelectric ceramics, Journal of the American Ceramic Society 93 (2010) 1108–1113.

[5] X. Tan, E. Aulbach, W. Jo, T. Granzow, J. Kling, M. Marsilius, H.J. Kleebe, J. Rödel, Effect of uniaxial stress on ferroelectric behavior of $(Bi_{1/2}Na_{1/2})TiO_3$-based lead-free piezoelectric ceramics, Journal of Applied Physics 106 (2009) 044107.

[6] T. Takenaka, K. Maruyama, K. Sakata, $Bi_{1/2}Na_{1/2})TiO_3$–$BaTiO_3$ system for lead-free piezoelectric ceramics, Japanese Journal of Applied Physics 30 (1991) 2236–2239.

[7] B.J. Chu, J.H. Cho, Y.H. Lee, B.I. Kim, D.R. Chen, The potential application of BNT-based ceramics in large displacement actuation, Journal of Ceramic Processing Research 3 (2002) 231–234.

[8] X.M. Chen, X.X. Gong, T.N. Li, Y. He, P. Liu, Microstructure, dielectric and ferroelectric properties of $(1-x)(0.94Bi_{0.5}Na_{0.5}TiO_3$–$0.06BaTiO_3)$–$xBiFeO_3$ lead-free ceramics synthesized via a high energy ball milling method, Journal of Alloys and Compounds 507 (2010) 535–541.

[9] X.M. Chen, W.Y. Pan, H.H. Tian, X.X. Gong, X.B. Bian, P. Liu, Microstructure, dielectric and ferroelectric properties of $0.94Bi_{0.5}Na_{0.5}TiO_3$–$0.06BaTiO_3$ (NBTB) and $0.05BiFeO_3$–0.95NBTB ceramics: effect of sintering atmosphere, Journal of Alloys and Compounds 509 (2011) 1824–1829.

[10] X.M. Chen, H.Y. Ma, W.Y. Pan, M. Pang, P. Liu, J.P. Zhou, Microstructure, dielectric and ferroelectric properties of $(Na_x$-$Bi_{0.5})_{0.94}Ba_{0.06}TiO_3$ lead-free ferroelectric ceramics: effect of Na nonstoichiometry, Materials Chemistry and Physics 132 (2012) 368–374.

[11] S.T. Zhang, A.B. Kounga, E. Aulbach, Giant strain in lead-free piezoceramics $Bi_{0.5}Na_{0.5}TiO_3$–$BaTiO_3$–$K_{0.5}Na_{0.5}NbO_3$ system, Applied Physics Letters 91 (2007) 112906.

[12] F. Gao, X.L. Dong, C.L. Mao, F. Cao, G.S. Wang, c/a ratio-dependent energy-storage density in $(0.9-x)Bi_{0.5}Na_{0.5}TiO_3$–$xBaTiO_3$–$0.1K_{0.5}Na_{0.5}NbO_3$ ceramics, Journal of the American Ceramic Society 94 (2011) 4162–4164.

[13] W. Jo, E. Erdem, R. Eichel, J. Glaum, T. Granzow, D. Damjanovic, J. Rödel, Effect of Nb-donor and Fe-acceptor dopants in $(Bi_{1/2}Na_{1/2})$-TiO_3-$BaTiO_3$–$(K_{0.5}Na_{0.5})NbO_3$ lead-free piezoceramics, Journal of Applied Physics 108 (2010) 014110.

[14] Q. Xu, M. Chen, W. Chen, H.X. Liu, B.H. Kim, B.K. Ahn, Effect of CoO additive on structure and electrical properties of $(Na_{0.5}Bi_{0.5})_{0.93}$-$Ba_{0.07}TiO_3$ ceramics prepared by the citrate method, Acta Materialia 56 (2008) 642–650.

[15] X.P. Jiang, Y.Y. Zheng, F.L. Jiang, L.H. Liu, K.W. Kwok, H.L.W. Chan, Properties of Co-doped $0.92(Na_{0.5}Bi_{0.5})TiO_3$–$0.08BaTiO_3$ lead-free ceramics, Chinese Physics Letters 24 (2007) 3257–3259.

[16] H.C. Hu, M.K. Zhu, F.Y. Xie, N. Lei, J. Chen, Y.D. Hou, H. Yan, Effect of Co_2O_3 additive on structure and electrical properties of $85(Bi_{1/2}Na_{1/2})TiO_3$–$12(Bi_{1/2}K_{1/2})TiO_3$–$3BaTiO_3$ lead-free piezoceramics, Journal of the American Ceramic Society 92 (2009) 2039–2045.

[17] G. Picht, J. Töpfer, E. Hennig, Structural properties of $(Bi_{0.5}Na_{0.5})_{1-x}Ba_xTiO_3$ lead-free piezoelectric ceramics, Journal of the European Ceramic Society 30 (2010) 3445–3453.

[18] H.I. Hsiang, L.T. Mei, Y.J. Chun, Dielectric properties and microstructure of Nb-Co codoped $BaTiO_3$–$(Bi_{0.5}Na_{0.5})TiO_3$ ceramics, Journal of the American Ceramic Society 92 (2009) 2768–2771.

[19] J.G. Fisher, S.J.L. Kang, Microstructural changes in $(K_{0.5}Na_{0.5})NbO_3$ ceramics sintered in various atmospheres, Journal of the European Ceramic Society 29 (2009) 2581–2588.

[20] J.A. Zvirgzds, P.P. Kapostins, J.V. Zvirgde, T.V. Kruzina, X-ray study of phase transitions in ferroelectric $Na_{0.5}Bi_{0.5}TiO_3$, Ferroelectrics 40 (1982) 75–77.

[21] S.B. Vakhrushev, V.A. Isupov, B.E. Kvyatkovsky, N.M. Okuneva, I.P. Pronin, G.A. Smolensky, P.P. Syrnikov, Phase transitions and soft modes in sodium bismuth titanate, Ferroelectrics 63 (1985) 153–160.

[22] M.S. Zhang, J.F. Scott, Raman spectroscopy of $Na_{0.5}Bi_{0.5}TiO_3$, Ferroelectrics Letters 6 (1986) 147–152.

[23] J.K. Lee, J.Y. Yi, K.S. Hong, Dependence of incommensurate phase formation on vacancy type in La-doped $(Na_{1/2}Ba_{1/2})TiO_3$, Journal of Applied Physics 96 (2004) 1174–1177.

[24] J. Suchanicz, J. Kusz, H. Böhm, H. Duda, J.P. Mercurio, K. Konieczny, Structural and dielectric properties of $(Na_{0.5}Bi_{0.5})_{0.70}$-$Ba_{0.30}TiO_3$ ceramics, Journal of the European Ceramic Society 23 (2003) 1559–1564.

[25] X.X. Wang, X.G. Tang, H.L.W. Chan, Electromechanical and ferroelectric properties of $(Bi_{1/2}Na_{1/2})TiO_3$–$(Bi_{1/2}K_{1/2})TiO_3$–$BaTiO_3$ lead-free piezoelectric ceramics, Applied Physics Letters 85 (2004) 91–93.

[26] Y. Hiruma, H. Nagata, T. Takenaka, Transition temperatures and piezoelectric properties of $(Bi_{1/2}Na_{1/2})TiO_3$–$(Bi_{1/2}K_{1/2})TiO_3$–$BaTiO_3$ lead-free piezoelectric ceramics, Japanese Journal of Applied Physics 45 (2006) 7409–7412.

[27] Y. Hiruma, Y. Imai, Y. Watanabe, H. Nagata, T. Takenaka, Large electrostrain near the phase transition temperature of $(Bi_{0.5}Na_{0.5})$-TiO_3–$SrTiO_3$ ferroelectric ceramics, Applied Physics Letters 92 (2008) 262904.

[28] S.E. Park, S.J. Chung, I.T. Kim, Ferroic phase transitions in $Na_{0.5}BI_{0.5}TiO_3$ crystals, Journal of the American Ceramic Society 79 (1996) 1290–1296.

[29] S.W. Zhang, H.L. Zhang, B.P. Zhang, G.L. Zhao, Dielectric and piezoelectric properties of $(Ba_{0.95}Ca_{0.05})(Ti_{0.88}Zr_{0.12})O_3$ ceramics sintered in a protective atmosphere, Journal of the European Ceramic Society 29 (2009) 3235–3242.

[30] A. Tkach, P.M. Vilarinho, A.L. Kholkin, Dependence of dielectric properties of manganese-doped strontium titanate ceramics on sintering atmosphere, Acta Materialia 54 (2006) 5385–5391.

[31] Hari Singh Nalwa, Handbook of low and high dielectric constant materials and their applications, vol. 1, Academic Press, London, 1999.
[32] J.G. Fisher, D. Rout, K.S. Moon, S.J.L. Kang, Structural changes in potassium sodium niobate ceramics sintered in different atmospheres, Journal of Alloys and Compounds 479 (2009) 467–472.
[33] J.G. Fisher, D. Rout, K.S. Moon, S.J.L. Kang, High-temperature X-ray diffraction and raman spectroscopy study of $(K_{0.5}Na_{0.5})NbO_3$ ceramics sintered in oxidizing and reducing atmospheres, Materials Chemistry and Physics 120 (2010) 263–271.
[34] X.M. Chen, P. Liu, J.P. Zhou, W.W. Kong, J.W. Zhang, Structure and dielectric properties of $Ba(Ti_{0.99}Ni_{0.01})O_{3-\delta}$ ceramic synthesized via high energy ball milling method, Physica B-Condensed Matter 405 (2010) 2815–2819.
[35] K. Uchino, E. Sadanaga, T. Hirose, Dependence of the crystal structure on particle size in barium titanate, Journal of the American Ceramic Society 72 (1989) 1555–1558.
[36] S. Lee, C.A. Randall, Z.K. Liu, Modified phase diagram for the barium oxide-titanium dioxide system for the ferroelectric barium titanate, Journal of the American Ceramic Society 90 (2007) 2589–2594.
[37] K. Uchino, S. Nomura, Critical exponents of the dielectric constants in diffused-phase-transition crystals, Ferroelectrics 44 (1982) 55–61.
[38] Q. Xu, D.P. Huang, M. Chen, W. Chen, H.X. Liu, B.H. Kim, Effect of bismuth excess on ferroelectric and piezoelectric properties of a $(Na_{0.5}Bi_{0.5})TiO_3$–$BaTiO_3$ composition near the morphotropic phase boundary, Journal of Alloys and Compounds 471 (2009) 310–316.
[39] L.J. Liu, H.Q. Fan, S.M. Ke, X.L. Chen, Effect of sintering temperature on the structure and properties of cerium-doped $0.94(Bi_{0.5}Na_{0.5})TiO_3$–$0.06BaTiO_3$ piezoelectric ceramics, Journal of Alloys and Compounds 458 (2008) 504–508.
[40] W.R. Buessem, L.E. Cross, A.K. Goswami, Phenomenological theory of high permittivity in fine-grained barium titanate, Journal of the American Ceramic Society 49 (1966) 33–36.
[41] T. Friessnegg, S. Aggarwal, R. Ramesh, B. Nielsen, E.H. Poindexter, D.J. Keeble, Vacancy formation in $(Pb,La)(Zr,Ti)O_3$ capacitors with oxygen deficiency and the effect on voltage offset, Applied Physics Letters 77 (2000) 127–129.